

R. Kovacevic  
Mem. ASME

Y. M. Zhang  
Mem. ASME

S. Ruan

Center for Robotics and  
Manufacturing Systems and  
Department of Mechanical Engineering,  
University of Kentucky,  
Lexington, KY 40506

# Sensing and Control of Weld Pool Geometry for Automated GTA Welding

*Weld pool geometry is a crucial factor in determining welding quality, especially in the case of sheet welding. Its feedback control should be a fundamental requirement for automated welding. However, the real-time precise measurement of pool geometry is a difficult procedure. It has been shown that vision sensing is a promising approach for monitoring the weld pool geometry. Quality images that can be processed in real-time to detect the pool geometry are acquired by using a high shutter speed camera assisted with nitrogen laser as an illumination source. However, during practical welding, impurities or oxides existing on the pool surface complicate image processing. The image features are analyzed and utilized for effectively processing the image. It is shown that the proposed algorithm can always detect the pool boundary with sufficient accuracy in less than 100 ms. Based on this measuring technique, a robust adaptive system has been developed to control the pool area. Experiments show that the proposed control system can overcome the influence caused by various disturbances.*

## 1 Introduction

Sensing and control are important parts of welding automation. Early efforts [1-6] illustrated great potentials in sensing and closed-loop control for improving arc weld quality. Through recent developments [7-13], their perspective can be clearly seen.

To achieve good weld quality, several weldment characteristics should be sensed and controlled [13]. For implementation convenience, top-side sensors are frequently preferred. However, some weldment quality characteristics are difficult to detect from the topside. For example, the weld penetration is primarily described by the back-side bead width and depth of penetration for full penetration and partial penetration modes, respectively. These characteristics cannot directly be seen from the topside and, therefore, only indirect methods have been proposed. Thus, the top-side sensing of the weld quality is frequently indirect.

The weld pool is the key of arc welding and contains abundant information of the welding process. Its geometry, which can directly be observed from the topside, should be a crucial factor in determining the welding quality, especially in the case of sheet welding. However, due to the difficulty associated with the precise real-time measurement of weld pool geometry, its correlations with the weldment characteristics have not yet been fully experimentally determined. In our effort to improve welding quality through pool geometry sensing, both two-dimensional pool boundary sensing and three-dimensional pool surface shape sensing [14] have been

studied. The correlations between the pool geometry, two-dimensional and three-dimensional, and the weldment characteristics are currently under investigation.

An advanced two-dimensional pool geometry sensing and control technique is presented. It is apparent that the controlled parameters of pool geometry should be selected based on the required weldment characteristics and their correlations with the pool geometrical features. Although the precise real-time sensing of pool geometry developed in this paper can provide a fundamental technique for acquiring these correlations, long-term in-depth theoretical and experimental studies are required. It is noticed that so far control systems have been primarily developed based on pool width sensing. In our previous study [15], it was shown by GTAW of 3 mm-thick stainless steel plates that the weld width is not very sensitive to the variations in welding conditions. But, experiments on both .1 mm-thick and 3 mm-thick stainless steel show that the pool length is sensitive. Thus, the pool length should also be controlled.

To achieve a practical system, a simple system configuration is preferred. During automated or robotic welding, the torch trajectory (therefore, torch speed) is frequently preprogrammed. The arc length can be well maintained by arc length regulation. In this case, the welding current is often selected to regulate the welding process. The variations in current, heat transfer condition, material thickness, etc., which may be encountered during closed-loop control, will generate the same trends of variations for both the pool length and width. Thus, the variations in pool length and width can be approximately described by the variation of pool area. The pool area is, therefore, controlled to show the

Contributed by the Production Engineering Division for publication in the JOURNAL OF ENGINEERING FOR INDUSTRY. Manuscript received June 1993; revised April 1994. Associate Technical Editor: E. Kannatey-Asibu.

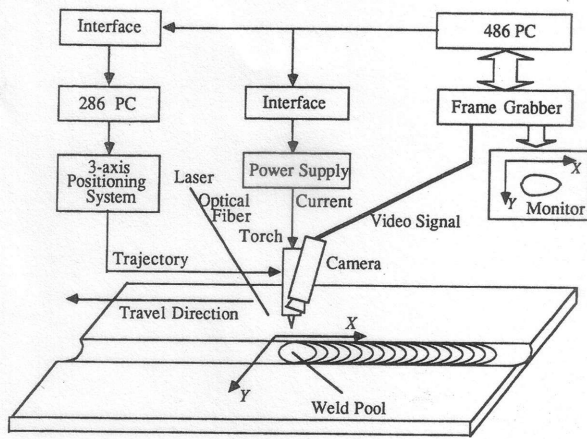


Fig. 1(a)

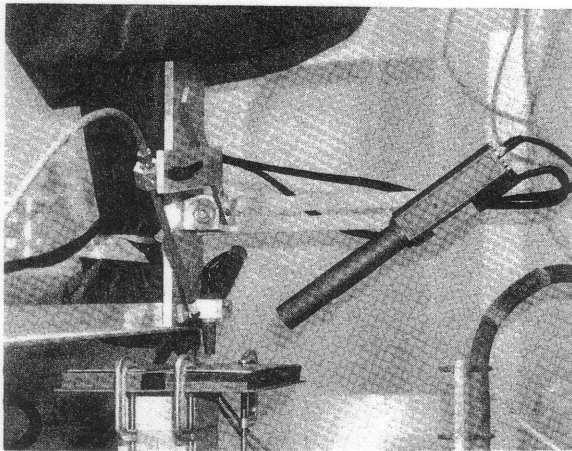


Fig. 1(b)

Fig. 1 Experimental set-up; (a) diagram, (b) photograph

perspective of the pool geometry sensing and control in acquiring quality welds.

## 2 Sensing System and Experimental Setup

Principally, weld pool geometry could be indirectly detected by pool oscillation [16, 17], ultrasonic sensing [18, 19], infrared sensing [10, 20], and radiography [21]. However, to obtain more precise measurement, the direct method, i.e., the vision based method, may be more promising. The co-axial viewing was proposed by Richardson [22] and has been extensively investigated by a number of researchers. Since the weld pool surface is mirror-like, the diffusion reflection of the arc light from the weld pool is weaker than that from the surrounding area. However, the intensity contrast of the pool against the surrounding area is low, due to the radiation from the pool. Even though excellent algorithms have been developed, it still requires 6.5 seconds, on a VAX 11/785 computer [23], or a few tens of seconds, on a 12 MHz 80286-based machine [24], in order to extract the pool edge from an ideal image, i.e., without oxides or impurities on the pool. For pool width, a real-time PID control system of 8 Hz has been developed [25]. However, when oxides or impurities existed, the algorithm failed [25].

In this study, we will improve the contrast between the weld pool and surrounding area by increasing the reflection from the solid area. To do this, a strong illumination must be projected onto the area of interest. The Control Vision ultra-high shutter speed vision system [26] is ideal for this application. This system consists of a strobe-illumination unit

(pulse laser), camera head and system controller. The pulse duration of the laser is 3 ns and the camera is synchronized with the laser pulse. Thus, the intensity of laser illumination is much higher than those of the arc and hot metal during the pulse duration. Using this vision system, good weld pool contrast can always be obtained under different welding conditions.

The experimental setup is illustrated in Fig. 1. The main computer (486 PC) controls the welding current, which regulates the pool area, through its interface to the power supply, a DC gas tungsten arc (GTA) welding machine. The torch trajectory, therefore, the torch speed and arc length, is controlled and preprogrammed by the 286 PC. The camera and laser are attached to and move with the torch in order to view the weld pool and its surrounding area. The resultant images are converted into the digital matrices by a  $512 \times 512$  8 bit frame grabber with resolutions  $\text{pixel}_x = 0.0277$  mm along the travel direction and  $\text{pixel}_y = 0.0406$  mm along the traversal direction (see Fig. 1(a)). (This has assumed a fixed relationship between the camera and travel directions. This assumed directional relationship can be maintained by rotating the manipulator during welding if the seam is not straight.) The main computer processes the images to obtain the pool edge and pool area, and then calculates the current required to realize the desired pool area through the adaptive feedback algorithm.

Some typical images of GTA weld pool captured using the above vision system are shown in Fig. 2. (The extracted pool boundaries are also displayed with the pools.) The image shown in Fig. 2(a) is an ideal case where the pool edge can be clearly identified and the pool is purely dark. In Fig. 2(b), the electrode reflection exists. When unmolten oxides or impurities exist, the pool's mirror-like reflectivity will be disturbed (Fig. 2(c)). (The algorithm for the pool width extraction proposed in [25] has failed in this case.) In Fig. 2(d), the current is large and the arc cannot be eliminated entirely. In Figs. 2(e)-(g), the complexity of the pool rear imaging is shown. To control the pool area, a reliable real-time algorithm must be proposed to extract the weld pool edge for all possible cases.

## 3 Real-Time Pool Edge Extraction

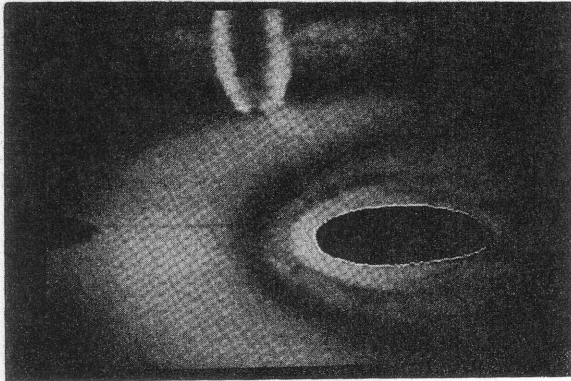
In this study, the torch speed is selected to be about 2 mm per second. In order to obtain fine control of weld pool area, the sampling interval along the seam must be small. For sheet welding, the pool geometry is more sensitive to variations in welding conditions than in the cases of plate and thick material welding. Thus, this interval is selected as 0.5 mm and, therefore, the corresponding time interval is 250 ms. Considering image acquisition and control calculation, an algorithm that can extract the weld pool edge and calculate its area in 150 ms is preferred. Such an algorithm can be regarded as real-time.

**3.1 Image Features.** To propose an effective algorithm, the image features must be analyzed. It can be seen that the grayness difference between the weld pool and its surrounding solid material appears as the most apparent feature of the image. The grayness values associated with the pool are low. Ideally, they should be zero except for oxide or impurity floats. However, in some cases the grayness varies significantly in the weld pool (see Fig. 2(d)). This variation is caused by the arc that has not been entirely eliminated from the image by the camera. In some cases, larger grayness may be found on the pool than on the solidified materials. It seems that the weld pool edge is difficult to identify only through the grayness. The directional gradient of grayness radially from an interior pool point may present another feature. It can be seen that the largest directional gradient

often occurs at the edge. However, the largest gradients may occur at the oxide or outside the pool as well. Also, at the pool rear, the directional gradients associated with the pool edge are often not the largest or even the second largest. Some solidified area may have the same low grayness (zero) as the pool. This is probably caused by incomplete solidification. Thus, discriminating between the pool edge and oxide will be difficult unless the continuity of the edge is used. However, this continuity is often broken (see Fig. 2(f)) although it can still be identified by a human. Also, the shape

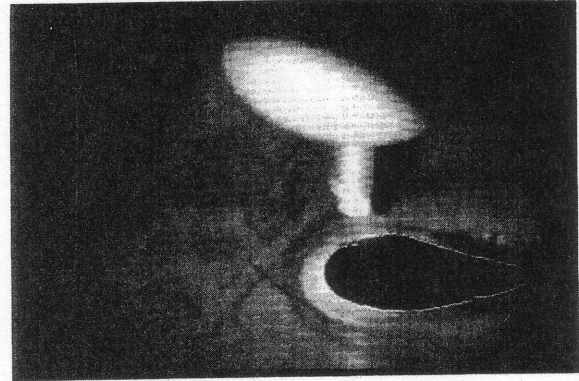
feature of the edge varies severely even under the same welding conditions.

It can be seen that the problem addressed is not pure edge detection. There are many edges other than the pool edge. Pattern recognition may be utilized to distinguish the pool edge from other edges, based on the continuity of pool edge. However, the computation for detecting all possible edges using standard algorithms [27] and then selecting the pool edge takes too much time to implement on-line. Still, no models can be easily presented for the pool edge description



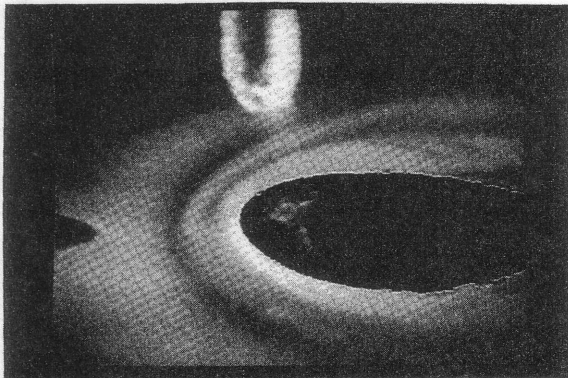
Current: 120 A Torch Speed: 3 mm/sec  
Arc length: 6 mm Stainless steel 304  
Argon rate: 15 L/min Workpiece: 250x 100x3 mm

Fig. 2(a)



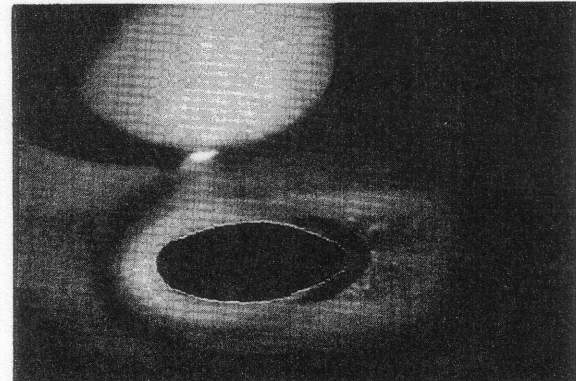
Current: 180 A Torch Speed: 4 mm/sec  
Arc length: 3 mm Stainless steel 304  
Argon rate: 10 L/min Workpiece: 250x 100x3 mm

Fig. 2(d)



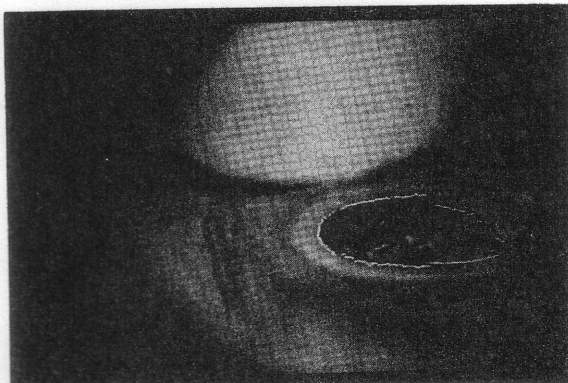
Current: 70 A Torch Speed: 2 mm/sec  
Arc length: 6 mm Stainless steel 304  
Argon rate: 15 L/min Workpiece: 250x 75x1 mm

Fig. 2(b)



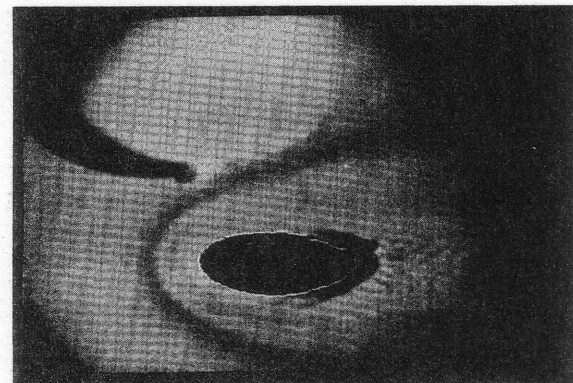
Current: 50 A Torch Speed: 2 mm/sec  
Arc length: 4 mm Stainless steel 304  
Argon rate: 10 L/min Workpiece: 250x 75x1 mm

Fig. 2(e)



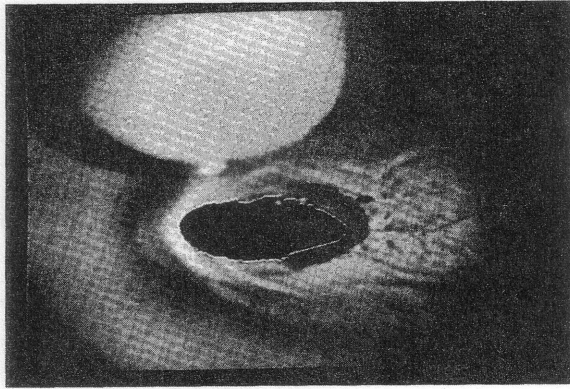
Current: 40 A Torch Speed: 2 mm/sec  
Arc length: 2.5 mm Stainless steel 304  
Argon rate: 8 L/min Workpiece: 250x 75x1 mm

Fig. 2(c)



Current: 35 A Torch Speed: 2 mm/sec  
Arc length: 4 mm Stainless steel 304  
Argon rate: 10 L/min Workpiece: 250x 75x1 mm

Fig. 2(f)



Current: 40 A Torch Speed: 2 mm/sec  
 Arc length: 2.5 mm Stainless steel 304  
 Argon rate: 8 L/min Workpiece: 250x75x1 mm

Fig. 2(g)

Fig. 2 Typical images and extracted pool boundaries; (a) ideal image, (b) with electrode reflection, (c) with oxide floats, (d) with large current, (e) complicated rear 1, (f) complicated rear 2, (g) complicated rear 3

because of the severe variation in shape. This complicates the possible application of model-based filters. Thus, it can be seen that an effective algorithm must be developed based on the utilization of the unique image features in combination with basic image processing concepts, rather than simply using exiting approaches. It seems that the pool edge extraction will be much more complicated than initially expected.

**3.2 Pool Edge Extraction.** Among the aforementioned image features, none can be used solely to identify the pool edge. In the proposed algorithm, different image features will be used. The pool edge is divided into three portions, i.e., the front edge, side (upper and lower) edges in the middle of the pool, and rear edge, in order to utilize their different features. Before identifying these portions, the weld pool must be located through finding a point of the weld pool.

(A) *Locating Pool:* A large area of low grayness in the illuminated area will be the pool area except for the possible incompletely-solidified range adjacent to the pool rear. Any point on this area, denoted as  $(x_0, y_0)$ , can be regarded as the point aforementioned. In order to exclude the possible small, low grayness areas caused by surface defects or uncleanliness, the target low grayness area must be sufficiently large. Thus, the following inequalities, in  $(x_0, y_0)$  and its eight components, is proposed to select  $(x_0, y_0)$ :

$$g(x_0 + i, y_0 + j) < g_0 \quad (i = 0, -\Delta_x, \Delta_x; j = 0, -\Delta_y, \Delta_y) \quad (1)$$

where  $g(x, y)$  is the grayness associated with the point  $(x, y)$ , and  $g_0$  is the low grayness threshold and selected to be  $g_0 = 0.2 g_m$  where  $g_m$  is the largest grayness encountered during the search which gradually increases before approaching the pool. Positive integers  $\Delta_x$  and  $\Delta_y$  should be selected based on possible size of surface defects. Experiments showed that  $\Delta_x = 5$  and  $\Delta_y = 5$  can always generate the required results in this study. The search process, in which the search step (i.e., 10) and search direction have been selected to reduce computation and avoid the influence of the dark area at the rear, is illustrated in Fig. 3.

(B) *Determining Front Edge:* The front edge always corresponds to the local maxima of the directional gradients radially from  $(x_0, y_0)$ . Thus, it is a continuous trajectory of local gradient maxima. However, the local maximum may not

be the largest gradient point, called the global maximum, because of the oxide floats, especially when the remaining arc reduces the gradient magnitude of the pool edge (Fig. 2(d)). This implies that the unique global maxima cannot be employed. The local maxima must be considered. However, along any line from  $(x_0, y_0)$ , several local maxima may exist. To select the correct one, additional features of the front edge must be incorporated.

The continuity of local maximum is an inherent feature associated with the edge of the pool front. This feature can be used to construct a dynamic algorithm for selecting the correct local maximum, i.e., the next edge point can be found based on the current edge point. The dynamic search can be done based on the dynamic thinning procedure (DTP) [9], along the search direction, i.e., the  $x$  or  $y$  direction, which is selected according to a rough estimate of the next edge point. Because only a small range is required to search dynamically, the computation can be significantly reduced. The oxide that floats on the pool even close to the edge can also be avoided. Thus, only the determination of the initial search point must be discussed.

Consider the three largest maxima on the axis  $x = x_0$  above  $(x_0, y_0)$ , denoted as  $(x_0, y_{u1})$ ,  $(x_0, y_{u2})$ , and  $(x_0, y_{u3})$  along the  $y$  direction according to their location (see Fig. 4). Also, suppose that  $(x_0, y_{b1})$ ,  $(x_0, y_{b2})$ , and  $(x_0, y_{b3})$  are the three largest maxima below  $(x_0, y_0)$  with  $y_0 \leq y_{b3} \leq y_{b2} \leq y_{b1}$  (see Fig. 4). It has been observed from experiments that the upper (lower) pool edge along the axis  $x = x_0$  is always one of  $(x_0, y_{uj})$ 's ( $j = 1, 2, 3$ ) ( $(x_0, y_{bj})$ 's ( $j = 1, 2, 3$ )). Thus, one of  $(x_0, y_{uj})$ 's ( $j = 1, 2, 3$ ) is the correct initial point for the dynamic search. To select the correct one, let us consider the three continuous trajectories of local maxima from  $(x_0, y_{uj})$ 's, denoted by  $c_i$  ( $i = 1, 2, 3$ ) respectively. If some  $c_i$  pass any of  $(x_0, y_{bj})$ , there must be corresponding physical existences on the image. For our problem, these possible existences must be the pool edge or oxide float as shown in Fig. 4. Thus, only the trajectories that pass one of  $(x_0, y_{bj})$ 's can be regarded as possible candidates for the front edge. Such  $c_i$ 's are said to be converged. If more than one candidate or converged  $c_i$  exist, the trajectory which has the largest  $D_i = (y_{bi} - y_{ui})$ , where  $(x_0, y_{bi})$  is passed by  $c_i$ , is the front edge. This trajectory is denoted by  $c_{i0}$  where  $D_{i0} = \max D_i$ . Consequently, the correct initial point and front edge trajectory can be acquired. For example, in Fig. 4,  $c_1$  and  $c_3$  are converged and  $c_1$  is the front edge.

(C) *Determining Side Edges:* The completion of the front edge search provides good initial points for the succeeding search. Assume that  $(x_0, y_u(x_0))$  and  $(x_0, y_b(x_0))$  are the upper and lower edge points, respectively. For the middle portion of the pool, the edge is also the continuous trajectory of local maxima. Thus, the following procedure is proposed according to the direction feature of the side edges:

(1) Detect the  $y$  coordinates of the pool edges in the range  $x_0 < x \leq x_0 + \Delta x$ , based on the DTP [9]. Here  $\Delta x$  determines the resolution of the division between the middle portion and rear portion. However, an exact division is not required. Thus,  $\Delta x = 10 \text{ pixel}_x$  is selected and experiments have shown that this selection always works. The resultant upper and lower edges are denoted as  $c_u$  and  $c_b$ , respectively.

(2) If both  $y_u(x_0 + \Delta x)$  and  $y_b(x_0 + \Delta x)$  equal one of the corresponding largest three maxima (i.e.,  $(x_0 + \Delta x, y_{ui})$ 's or  $(x_0 + \Delta x, y_{bi})$ 's) above or below  $(y_u(x_0) + y_b(x_0))/2$  at the axis  $x = x_0 + \Delta x$ ,  $c_u$  and  $c_b$  are regarded as converged. If  $c_u$  and  $c_b$  are converged, go to (1) with the updated initial parameters. Otherwise, begin the rear search.

Note that there are no exact boundaries for different portions of the weld pool. For the rear portion, the local maximum trajectory may not be continuous while it is in the

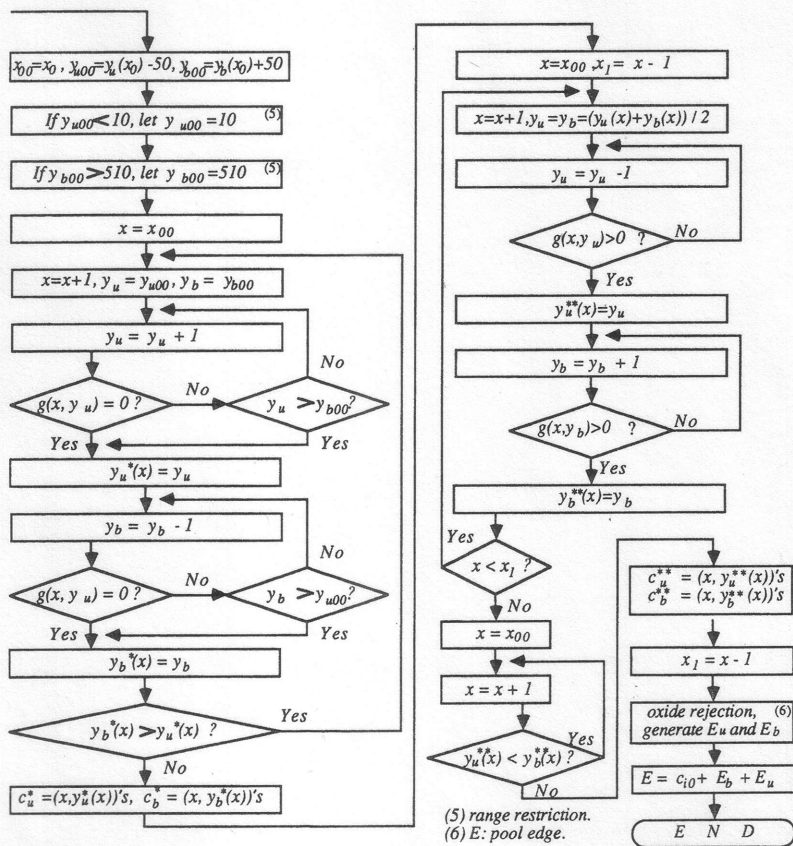
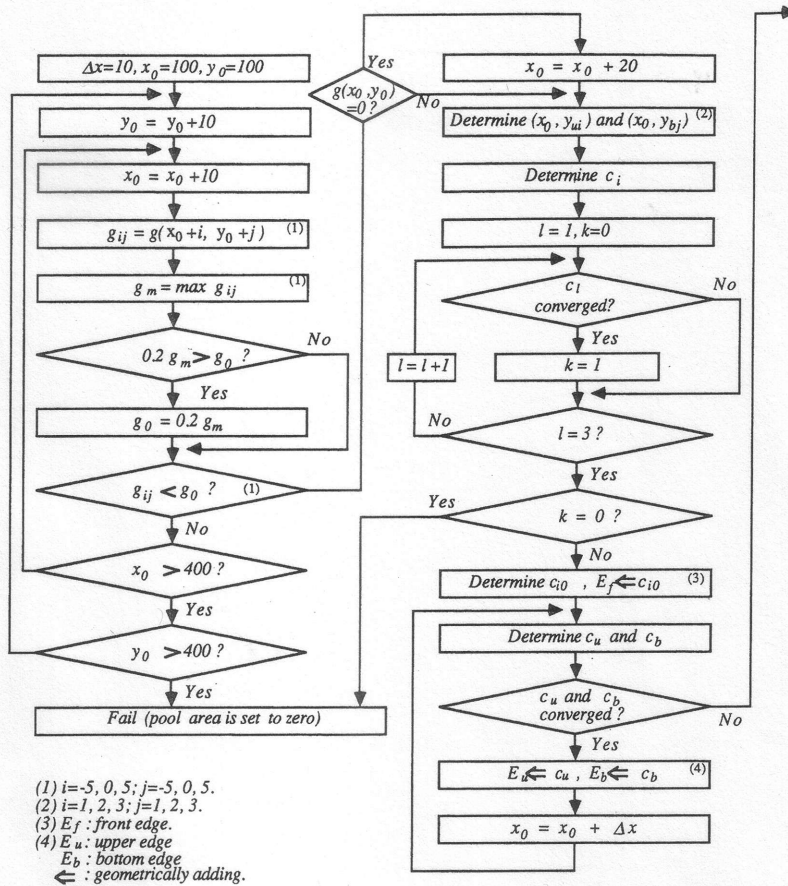


Fig. 3 Flow chart of edge detection

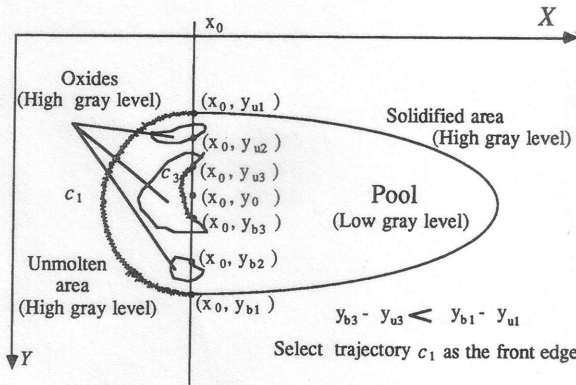


Fig. 4 Identification of front edge

middle portion. Based on this fact, different algorithms have been proposed for different portions. The condition for algorithm switching has also been designed accordingly.

(D) *Determining Rear Edge:* As has been shown, the imaging of the rear region is quite complicated due to the possible discontinuity of the local maxima and low grayness area adjacent to the pool rear (see Figs. 2(e)-(g)). Frequently, the grayness of this area is zero as on the pool. The features for distinguishing the edge fully disappear, except for the physical continuity of edge.

Since the gradients associated with the rear edge may be very small in some cases, the local maximum principle used in the middle and front portions may be difficult to apply. However, in the rear portion, the grayness of the pool is always low except for the oxides or impurities. (If the grayness outside the pool was always high like the solid area adjacent to the front and middle portions of pool, this low grayness might be an adequate condition for rear edge determination.) Thus, two different areas of low grayness must be distinguished. To do this, a three-step method is proposed. In the first step, the upper and lower boundaries of the low grayness range are searched from outside towards the pool marching along the  $x$  direction, denoted as  $c_u^*$  and  $c_b^*$ , respectively. If the lower and upper boundaries intersect, the first step search stops. Figure 5(a) illustrates  $c_u^*$  and  $c_b^*$ . It can be seen that the rear edge lies within the boundary  $c_u^*$  and  $c_b^*$ . The details of this step can be seen in Fig. 3.

In the second step, the search is performed from inside of the pool. The central line of  $c_u^*$  and  $c_b^*$  (see Fig. 5(a)) can be used as the search initial. Thus, the upper and lower boundaries of low grayness area can be searched again. These new boundaries are denoted as  $c_u^{**}$  and  $c_b^{**}$ , respectively (see Fig. 5(b)). The details for this search step can be seen in Fig. 3.

If no oxides or impurities exist in the pool rear,  $c_u^{**}$  and  $c_b^{**}$  will be the rear edge. However, the assumption that no oxides or impurities exist is unrealistic. Thus, an oxide rejection approach is proposed as the third step. First, the possible largest oxide length, denoted as  $L_m$ , along the  $x$  axis can be assumed. (Note: if an oxide is too long compared with the rear portion of the pool, the proposed oxide rejection algorithm may not work properly. In this case, an alternative algorithm will be required. However, in our case, even if the surface is not treated, such a large oxide has not been found in extensive experiments.) For the  $c_u^{**}$  segments which equal the corresponding  $c_u^*$  segments, it can be assumed that no oxides were encountered, thus these segments are taken as the pool edge. For the segments that are distinct from  $c_u^*$ , we should further judge if these segments include the oxide edge. The approach is:

(1) If the segment length along the  $x$  axis is less than  $L_m$ , the difference between  $c_u^{**}$  and  $c_u^*$  is caused by the oxide and the corresponding  $c_u^*$  segment is taken as the pool edge.

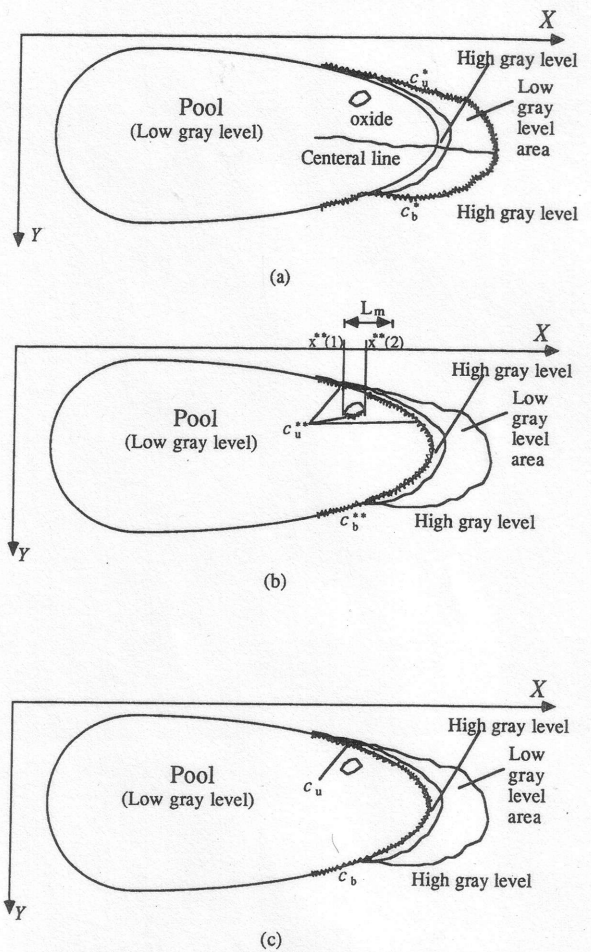


Fig. 5 Identification of rear edge; (a) first search, (b) second search, (c) final edge

(2) If the segment length along the  $x$  axis is larger than  $L_m$ , find the largest  $d(1) = y_u^{**}(x) - y_u^{**}(x-1)$  and  $d(2) = y_u^{**}(x) - y_u^{**}(x+1)$  and their corresponding  $x$  coordinates  $x^{**}(1)$  and  $x^{**}(2)$  (see Fig. 5(b)). At any  $x \in [x^{**}(1), x^{**}(2)]$ , the search for the next bright range edge can be performed for the new  $c_u^{**}$ . (To do this, one bright range ( $g \geq 1$ ) and one dark range ( $g = 0$ ) must first be passed. The succeeding bright range edge is just the new  $c_u^{**}$ .) If  $d(1) + d(2)$  is reduced, it can be assumed that the range  $[x^{**}(1), x^{**}(2)]$  contains oxides and the new bright range edge points can be used to modify  $c_u^{**}$ . And the above procedure can be repeated. Otherwise, the previous  $c_u^{**}$  are taken as the rear edge.

For the lower edge, the oxide rejection can be done similarly. Thus, through the proposed oxide rejection approach, the oxide edge portion of  $c_u^{**}$  in Fig. 5(b) can be rejected and the rear edge as shown in Fig. 5(c) can be acquired.

Based on the above discussion on the pool edge extraction algorithm, its flow chart as shown in Fig. 3 can be obtained. Once the edge is extracted, the pool area can be calculated directly from the edge points' coordinates as a sum of three integrals, i.e., front, middle, and rear area integrals along the respective direction, along that the dynamic search for the edge points were performed. If a very fine pool boundary is required, a finer search can be conducted based on the extracted pool edge with no directional restrictions, with little additional computation.

It should be pointed out that our algorithm for pool boundary detection was proposed based on collected images. It seems impractical to reveal all possible patterns of images

through a theoretical analysis and then propose a perfect algorithm. In this study, extensive images have been processed on-line during welding. The extracted pool boundaries are displayed on the monitor. It has been observed that the proposed algorithm always works well under different conditions (see Fig. 2 where the extracted pool boundaries are shown with the original images). Also, the total time for edge

Consider the  $k$ th instant. The least squares estimate of  $a$  and  $b$  with a forgetting factor  $\rho$  ( $0 < \rho \leq 1$ ) is denoted by  $a(k)$  and  $b(k)$ . It can be shown that [28]:

$$(a(k), b(k))^T = A^{-1}(k)B(k) \quad k \geq 2 \quad (3)$$

where  $A(k)$  and  $B(k)$  are recursively calculated by the following equations:

$$\begin{cases} A(k) = \rho A(k-1) + \begin{bmatrix} s^2(k-1) & s(k-1)i(k-1) \\ s(k-1)i(k-1) & i^2(k-1) \end{bmatrix} \\ B(k) = \rho B(k-1) + \begin{bmatrix} s(k-1)s(k) \\ i(k-1)s(k) \end{bmatrix} \end{cases} \quad k \geq 1 \quad (4)$$

extraction and area computation is less than 100 ms. For our problem, this speed can be regarded as real-time.

#### 4 Robust Adaptive Control

It is known that for sheet welding, the weld pool size is very sensitive to variations in the welding conditions or parameters. If resultant variations in the system dynamics can be identified through on-line data, an adaptive control, the promise of which in complicated welding process control has been shown by extensive studies at the MIT [12, 13], can be used to improve the control performances.

**4.1 Dynamic Model.** In digital control, the dynamic system is frequently described by an ARMA model [28]. To identify the model, dynamic experiments have been performed under typical welding conditions. The experimental data is processed by the Least Squares algorithm [28] and the AIC criteria [29] for parameter estimation and order selection. It has been shown, for addressed typical welding conditions, that the system models are ARMA (1, 1):

$$s(k) = as(k-j) + bi(k-j) + \epsilon(k) \quad (2)$$

where  $s(k)$  is the weld pool area at the  $k$ th sampling instant,  $i(k)$  is the current which is calculated at the  $k$ th sampling instance,  $a$  and  $b$  are the model parameters which vary with the welding conditions, and  $\epsilon(k)$  is the model residual.

**4.2 Adaptive Predictive Control.** Among accepted adaptive algorithms, the predictive ones have been widely accepted as very good robust controllers. The well-known generalized predictive control (GPC) [30] falls into this type of adaptive controller. Its successful applications can be seen in different areas in the literature. In our study, the predictive control is employed. The control algorithm parameters, including the smoothing factor  $\alpha$ , minimum costing horizon  $N_1$ , maximum costing horizon  $N_2$ , control horizon  $NU$ , and control weight  $\lambda$  [30] are selected to be 0.9, 1, 5, 1, and 0, respectively, based on the system dynamics, simulation and experimentation. The resultant control law can be obtained from Eq. (20) in Part I of [30], by using the above parameters, and the system model parameters (i.e.,  $C(q^{-1}) = 1$ ,  $A(q^{-1}) = 1 - aq^{-1}$ , and  $B(q^{-1}) = bq^{-1}$  where  $q^{-1}$  is the back-shift operator [30]) obtained from the on-line identifier.

**4.3 On-Line Identifier.** The recursive least square algorithm with forgetting factor [28] has been widely applied in adaptive control practices. This approximation algorithm was proposed to eliminate the matrix inverting calculation. In our case, the duration of the welding process for a single path of weld is often short compared with many industrial processes to which adaptive control has been applied. To acquire accurate parameters estimates rapidly, an exact algorithm will be used.

with the initial values:

$$\begin{cases} A(0) = 0 \\ B(0) = 0 \end{cases}$$

It can be shown that the invertibility of  $A(k)$  is guaranteed in our case if  $k \geq 2$ . Since the dimensions associated with  $A$  are only  $2 \times 2$ , the computational burden of inverting it is very small. Thus, exact least squares estimates can be obtained with a slight additional computational burden.

When  $k$  is very small, the accuracy of the above estimates may not be sufficient. The useful initial parameters should be used to improve the accuracy. The following logic has been utilized to generate  $a$  and  $b$  for the prediction control:

$$(a, b)^T = \gamma(a, b)^T + (1 - \gamma)(a(k), b(k))^T \quad (5)$$

where  $\gamma$  can be selected in the range between 0 and 1. Thus, an adaptive controller associated with the on-line parameter estimator can be implemented.

The above on-line identifier is developed based on the so called difference model which is used in digital control practices. However, when this on-line identifier is incorporated into the adaptive control, oscillation is frequently observed. Fig. 6(a) illustrates the output response using such an on-line identifier. The identified  $a$  and  $b$  are also plotted. It can be seen that the parameters fluctuate severely (see Figs. 6(b) and (c)). In this case, the workpiece width is constant along the seam. The parameters should not vary in such large ranges. To analyze the cause, the details within the sampling period must be studied.

The logic within sampling periods is shown in Fig. 7. At  $t = t(k)$ , the computer sends the sampling command to the frame grabber. However, the actual sampling instant will be  $t_s(k)$ . The difference between  $t(k)$  and  $t_s(k)$  depends on the camera status. After image converting and processing, the pool area can be calculated. This area is denoted as  $s(k)$ . It is apparent that  $s(k)$  is the area at  $t = t_s(k)$ . The new current based on  $s(k)$  is obtained and sent at  $t_i(k)$ . This current is denoted by  $i(k)$ . In the above adaptive control,  $s(k)$  and  $i(k)$  have been used as the area and current at the sampling instant  $k$  as commonly practiced in digital control. However, since  $(t_i(k) - t_s(k))$  occupies a significant percentage of a sampling period, this common practice is not appropriate in our case. Thus, consider the following first-order differential equation:

$$\frac{ds}{dt} = c_0 s + c_1 i \quad (6)$$

where  $c_0$  and  $c_1$  are model parameters. The difference approximation of this differential equation is:

$$s(t) - s(t_0) = c_0 s(t_0)(t - t_0) + c_1 \int_{t_0}^t i(t) dt \quad (7)$$

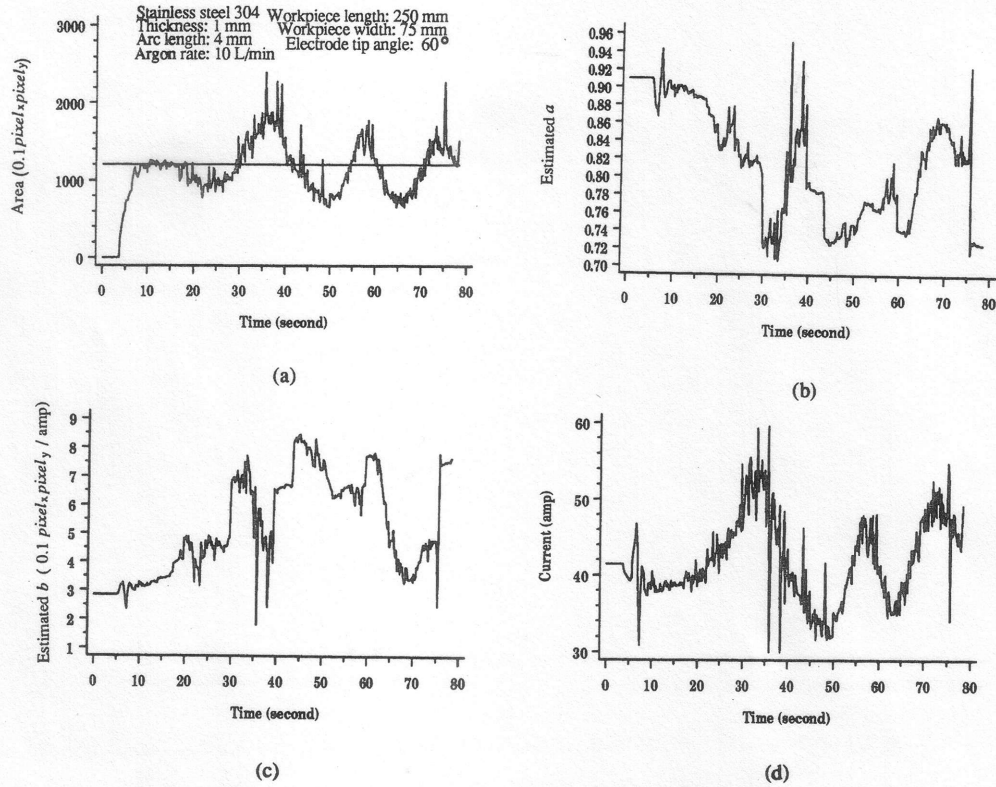


Fig. 6 Experiment using common on-line identification; (a) measured pool area, (b) identified parameter  $a$ , (c) identified parameter  $b$ , (d) welding current

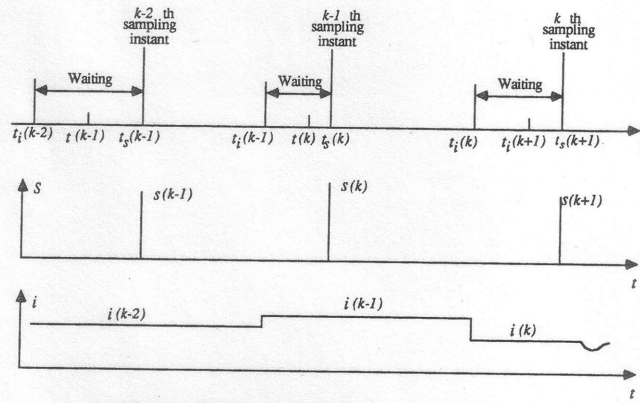


Fig. 7 Timing logic with sampling periods

Hence,

$$s(k) = (1 + c_0(t_s(k) - t_s(k-1)))s(k-1) + c_1(i(k-1)(t_s(k) - t_i(k-1)) + i(k-2)(t_i(k-1) - t_s(k-1))) \quad (8)$$

Assume that the sampling period is  $\Delta T$ . Then

$$s(k) = (1 + \tilde{c}_0\Delta T)s(k-1) + \tilde{c}_1(T_1i(k-1) + T_2i(k-2)) \quad (9)$$

where

$$\tilde{c}_0 = c_0(t_s(k) - t_s(k-1))/\Delta T$$

$$\tilde{c}_1 = c_1\Delta T$$

$$T_1 = (t_s(k) - t_i(k-1))/\Delta T$$

$$T_2 = (t_i(k-1) - t_s(k-1))/\Delta T$$

It can be seen that if  $T_2 = 0$  and  $\tilde{c}_0 = \text{constant}$ , the above equation will actually be the same as the difference equation (2). However,  $(t_s(k) - t_s(k-1))$  is not exactly equal to  $\Delta T$ . Also,  $T_2$  is frequently even larger than  $T_1$ . Thus, the description of (2) is not appropriate for on-line identification, and therefore fluctuating parameter estimates are produced. This problem can be solved by using the following equation for on-line identification:

$$\tilde{s}(k) = \tilde{a}s(k-1) + \tilde{b}i(k-1) \quad (10)$$

where

$$\tilde{s}(k) = s(k) - s(k-1)$$

$$\tilde{i}(k-1) = T_1i(k-1) + T_2i(k-2)$$

The on-line identification scheme for (10) is similar to that for (2). That is:

$$(\tilde{a}(k), \tilde{b}(k))^T = \tilde{A}^{-1}(k)\tilde{B}(k) \quad k \geq 2$$

$$\begin{cases} \tilde{A}(k) = \rho\tilde{A}(k-1) + \begin{bmatrix} s^2(k-1) & s(k-1)\tilde{i}(k-1) \\ s(k-1)\tilde{i}(k-1) & \tilde{i}^2(k-1) \end{bmatrix} \\ \tilde{B}(k) = \rho\tilde{B}(k-1) + \begin{bmatrix} s(k-1)\tilde{s}(k) \\ \tilde{i}(k-1)\tilde{s}(k) \end{bmatrix} \end{cases} \quad k \geq 1$$

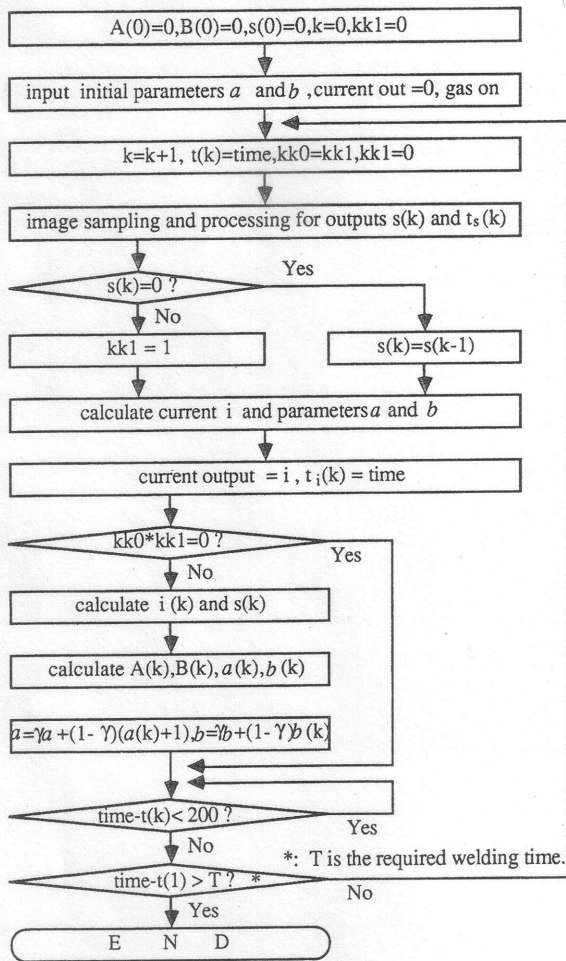


Fig. 8 Flow chart of adaptive control

$$\begin{cases} \tilde{A}(0) = 0 \\ \tilde{B}(0) = 0 \end{cases}$$

Once  $\tilde{a}$  and  $\tilde{b}$  are acquired,  $a$  and  $b$  can be obtained through:

$$a = \tilde{a} + 1, \quad b = \tilde{b}$$

Figure 8 is the flow chart of the proposed adaptive control algorithm. The diagram of the control system is illustrated in Fig. 9. The forgetting factor  $\rho$  and  $\gamma$  in Eq. (5) are taken as 0.97 and 0.91 throughout the experiments.

## 5 Experiment

To confirm the effectiveness of the proposed control system (a combination of the sensor, image processing and control algorithm), a variety of experiments have been conducted for initial parameters, torch speed variation and heat transfer condition change.

The experiments were done using the DC GTA welding with argon shielding and tungsten electrode ( $\phi 2.4$  mm). Since precision control of the welding process is primarily applied for generating high quality welds, stainless steel 304 is selected as the workpiece material. Also, for practical application, no care has been taken to clean the sheet surface. The sheet thickness is 1 mm. The torch speed is 2 mm/sec except for the speed change experiments.

**5.1 Initial Parameter.** The control algorithm calculates the welding current according to the plant dynamic model

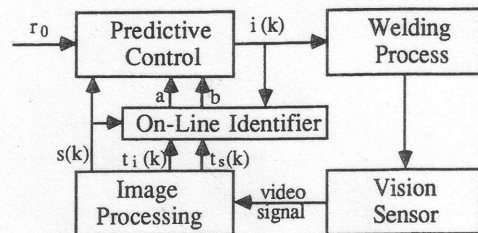


Fig. 9 Diagram of adaptive control system

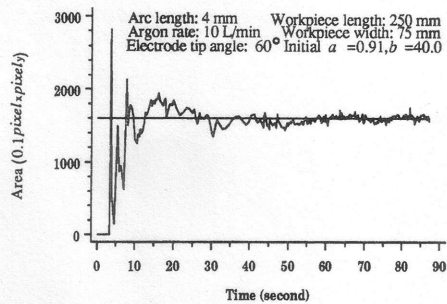
and the pool area measurements. Although the structure of the dynamic model is unified, the parameters depend on the welding conditions. Inaccurate parameters may not generate the required pool area. As the welding proceeds, accurate parameters can be obtained through on-line identification. However, at the beginning of welding, the required pool area cannot be acquired. The time required to obtain accurate parameters depends on the difference between the initial parameters and the actual parameters, and decreases as the accuracy of the initial parameters improves.

When the proposed control system is applied, the initial parameters of the dynamic model for each welding can be obtained from the last previous welding. Since the welding conditions may vary along the seam, the on-line identified parameters will also vary. Thus, the identified parameters at the beginning of the last previous welding should be selected as the initial parameters. With the consideration of identification convergency, the identified parameters at  $t = 40$  seconds are taken in our experiments.

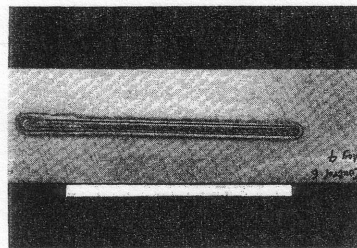
If the welding conditions of the present welding are the same as in the last welding, the above selection should generate proper initial parameters, which combined with the accurate measurements of the weld pool can improve the control performance. Thus, when the welding job is changed, only one trial is needed to guarantee the control performance. This trial is a self-learning process. However, for other control approaches, several trials may be required and the trial data must be analyzed to design the control algorithm again.

In the experiment shown by Fig. 10, improper initial parameters are used. Thus, at the beginning, the required pool area cannot be acquired. The overshooting is observed. After a period of about 37 seconds, the required pool area is obtained due to the on-line identification. Through this experiment, proper initial parameters for the dynamic model can be selected. Thus, the transition period is reduced to about 15 seconds (see Fig. 11). The satisfactory control effect is therefore realized.

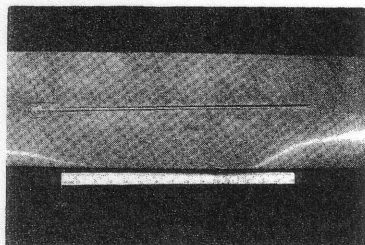
**5.2 Speed Change.** Even though a severe unexpected variation in torch speed may not be normal during automated and robotic welding where the torch speed is preprogrammed, this group of experiments are still arranged to emulate a large variation in welding conditions and test the system. In this group of experiments, the torch speed is changed from 2.5 mm/sec to 1.67 mm/sec at 62.5 mm from the beginning, i.e., at  $t = 25$  seconds. As a result, the weld size increases accordingly in the open-loop control (see Fig. 12(a)-(c)). The experimental results of the closed-loop control are illustrated in Fig. 13. It can be seen that when the welding begins, the desired pool size is quickly reached and maintained at the required level (see Fig. 13(a)). When the speed is changed to 1.67 mm/sec, the pool size increases. However, the control algorithm decreases the current accordingly (see Fig. 13(d)). Thus, the pool size is rapidly maintained at the desired level again. From the welding current signal, it can be seen that the control algorithm's response to the speed change is proper and fast.



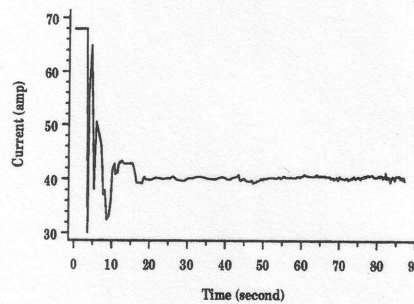
(a)



(b)

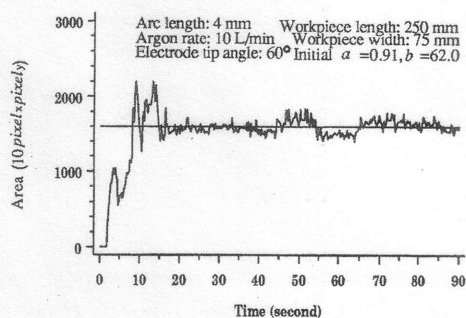


(c)

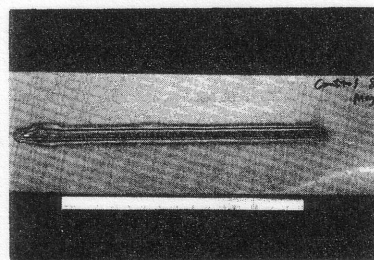


(d)

Fig. 10 Welding with improper initial parameters; (a) measured pool area, (b) top-side photograph, (c) back-side photograph, (d) welding current



(a)



(b)

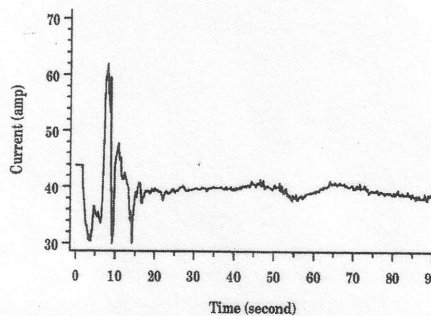
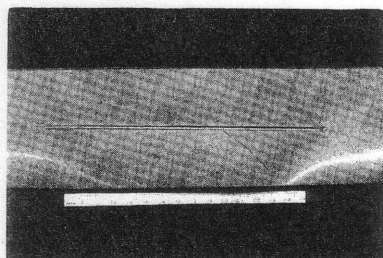
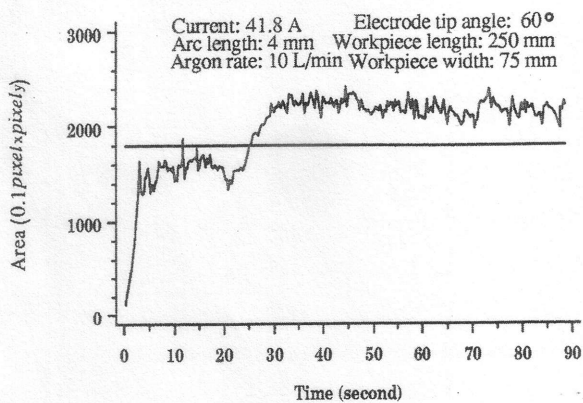


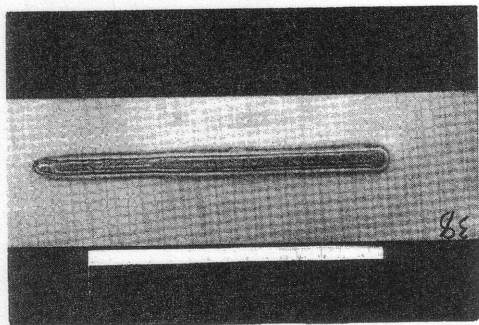
Fig. 11 Welding with proper initial parameters; (a) measured pool area, (b) top-side photograph, (c) back-side photograph, (d) welding current

It can also be seen from Fig. 13 that during approximately the last 25 seconds, unexpected variations in system dynamics occur. However, the control algorithm still maintains the pool size close to the desired level.

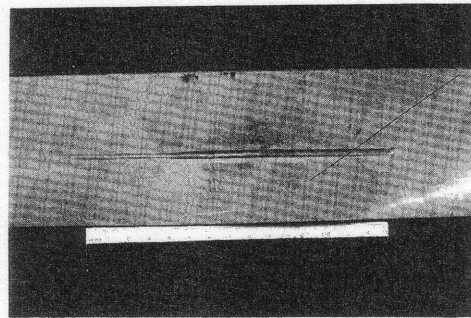
**5.3 Heat Transfer Condition Variation.** Non-constant heat transfer condition may be caused by the variations in workpiece structure, environmental temperature, pre-heating temperature, fixturing, etc. It is one of the major contributing



(a)



(b)

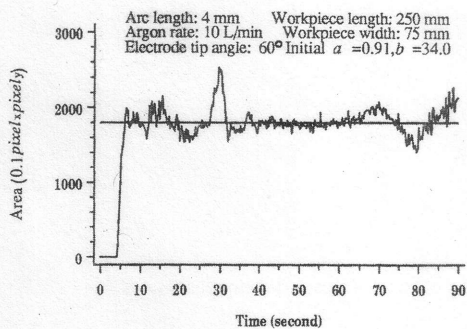


(c)

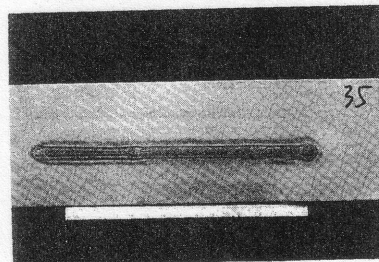
factors to varying pool size. In this group of comparative experiments, the heat transfer condition variation is emulated through the workpiece geometry (see Figs. 14 and 15). The experimental results associated with the open-loop control are illustrated in Fig. 14. It can be seen that the pool area, top-side bead width, and back-side bead width are significantly influenced by the heat transfer condition. However, the developed control system can maintain the required pool area (see Fig. 15(a) and (b)). Thus, the influence of the heat transfer condition on the back-side bead width is also eliminated (see Fig. 15(c)).

## 6 Conclusions

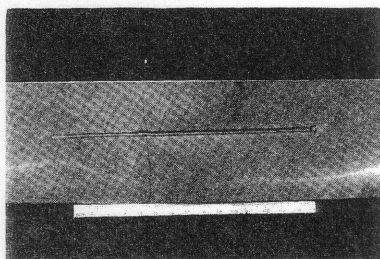
The high shutter speed camera with pulsed-laser illumina-



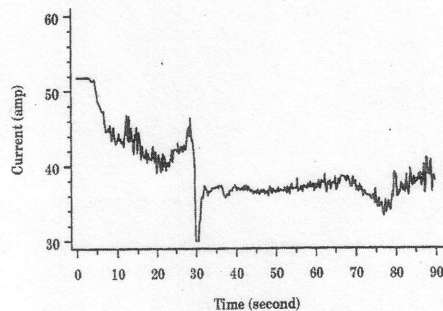
(a)



(b)

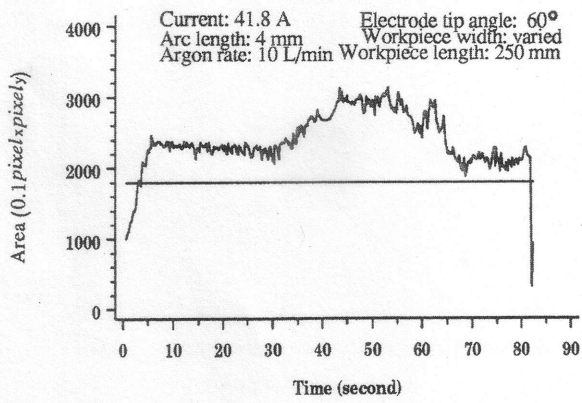


(c)

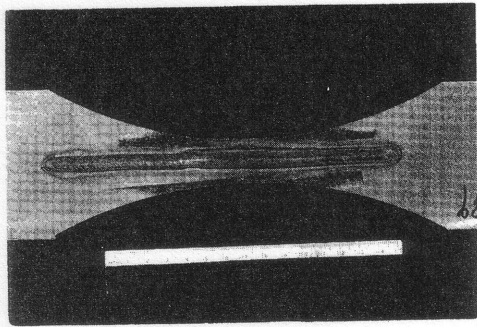


(d)

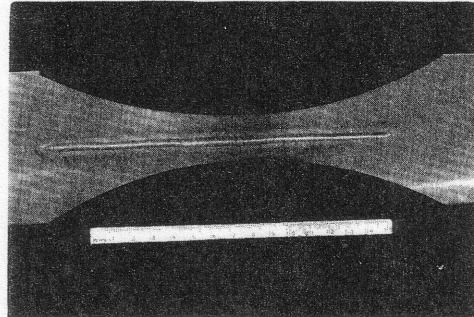
Fig. 13 Welding under speed change with proposed adaptive control system; (a) measured pool area, (b) top-side photograph, (c) back-side photograph, (d) welding current



(a)

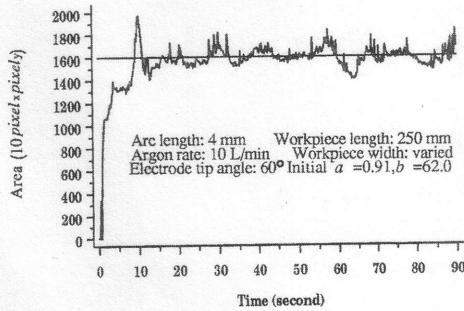


(b)

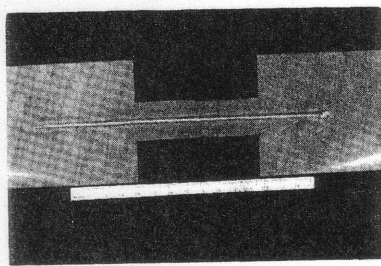


(c)

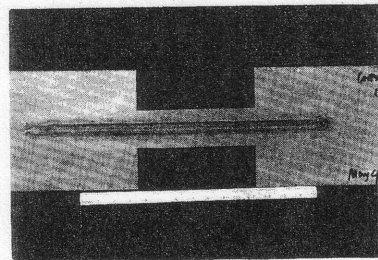
Fig. 14 Welding under varied heat transfer condition with open-loop control; (a) measured pool area, (b) top-side photograph, (c) back-side photograph



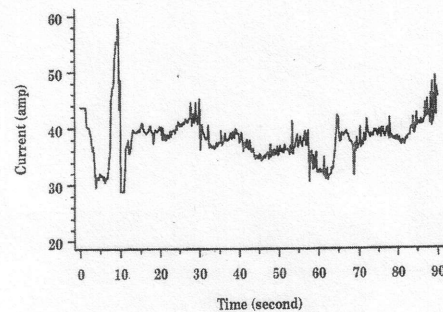
(a)



(b)



(c)



(d)

Fig. 15 Welding under varied heat transfer condition with proposed adaptive control system; (a) measured pool area, (b) top-side photograph, (c) back-side photograph, (d) welding current

niques, is capable of controlling the pool area under varied welding conditions.

### Acknowledgment

The financial support of the Control Vision Inc. and the Center for Robotics and Manufacturing Systems, University of Kentucky is greatly appreciated.

### References

- 1 Bennett, A. P., 1974, "The Interaction of Material Variability upon Process Requirements in Automatic Welding," *Advances in Welding Processes*, WI.
- 2 Vorman, A. R., and Brandt, H., 1976, "Feedback Control of GTA Welding Using Puddle Width Measurement," *Welding Journal*, Vol. 55, No. 9, pp. 742-749.
- 3 Hunter, J. J., Bryce, G. W., and Doherty, J., 1980, "On-line Control of the Arc Welding Process," *Developments in Mechanized Automated and Robotic Welding*, WI.
- 4 Dornfeld, D. A., Tomizuka, M., and Langari, G., 1982, "Modelling and Adaptive Control of Arc-Welding Processes," *Measurement and Control for Batch Manufacturing*, D. Hardt, ed., pp. 65-75, Nov.
- 5 Hardt, D. E., Garlow, D. A., and Weinert, J. B., 1985, "A Model of Full Penetration Arc-Welding for Control System Design," *ASME Journal of Dynamic Systems, Measurement, and Control*, Vol. 107, No. 1, pp. 40-46.
- 6 Bates, B. E., and Hardt, D. E., 1985, "A Real-Time Calibrated Thermal Model for Closed-Loop Weld Bead Geometry Control," *ASME Journal of Dynamic Systems, Measurement, and Control*, Vol. 107, No. 1, pp. 25-33.
- 7 Song, J.-B., and Hardt, D. E., 1993, "Closed-Loop Control of Weld Pool Depth Using a Thermally Based Depth Estimator," *Welding Journal*, Vol. 72, No. 10, pp. 471s-478s.
- 8 Zhang, Y. M., et al., 1993, "Determining Joint Penetration in GTAW with Vision Sensing of Weld-Face Geometry," *Welding Journal*, Vol. 72, No. 10, pp. 463s-469s.
- 9 Zhang, Y. M., Kovacevic, R., and Wu, L., 1993, "Closed-Loop Control of Weld Penetration Using Front-Face Vision Sensing," *Proc. Instn. Mech. Engrs., Part I, Journal of System and Control Engineering*, Vol. 207, No. 1, pp. 27-34.
- 10 Nagarajan, S., Banerjee, P., Chen, W. H., and Chin, B. A., 1992, "Control of the Welding Process using Infrared Sensors," *IEEE Transactions on Robotics and Automation*, Vol. 8, No. 1, pp. 86-93.
- 11 Liu, T., Cook, G. E., Barnett, R. J., and Springfield, J. F., 1992, "PC-based Arc Ignition and Arc Length Control System for Gas Tungsten Arc Welding," *IEEE Transactions on Industry Applications*, Vol. 28, No. 5, pp. 1160-1165.
- 12 Suzuki, A., Hardt, D. E., and Valavatt, L., 1991, "Application of Adaptive Control Theory to On-line GTA Weld Geometry Regulation," *ASME Journal of Dynamic Systems, Measurement, and Control*, Vol. 113, No. 1, pp. 93-103.
- 13 Doumanidis, C. C., and Hardt, D. E., 1991, "Multivariable Adaptive Control of Thermal Properties during Welding," *ASME Journal of Dynamic Systems, Measurement, and Control*, Vol. 113, No. 1, pp. 82-92.
- 14 Kovacevic, R., Zhang, Y. M., and Ruan, S., 1993, "Three-dimensional Measurement of Weld Pool Surface," *Proceedings of International Conference on Modeling and Control of Joining Processes*, Dec. 8-10, 1993, Orlando, FL.
- 15 Zhang, Y. M., Kovacevic, R., and Wu, L., 1992, "Sensitivity of Front-Face Weld Geometry in Representing the Full Penetration," *Proc. Instn. Mech. Engrs., Part B, Journal of Engineering Manufacture*, Vol. 206, No. 3, pp. 191-197.
- 16 Zacksenhouse, M., and Hardt, D. E., 1983, "Weld Pool Impedance Identification for Size Measurement and Control," *ASME Journal of Dynamic Systems, Measurement and Control*, Vol. 105, No. 3, pp. 179-184.
- 17 Renwick, R. J., and Richardson, R. W., 1983, "Experimental Investigation of GTA Weld Pool Oscillations," *Welding Journal*, Vol. 62, No. 2, pp. 29s-35s.
- 18 Hardt, D. E., and Katz, J. M., 1984, "Ultrasonic Measurement of Weld Penetration," *Welding Journal*, Vol. 63, No. 9, pp. 273s-281s.
- 19 Carlson, N. M., and Johnson, J. A., 1988, "Ultrasonic Sensing of Weld Pool Penetration," *Welding Journal*, Vol. 67, No. 11, pp. 239s-246s.
- 20 Chen, W., and Chin, B. A., 1990, "Monitoring Joint Penetration using Infrared Sensing Techniques," *Welding Journal*, Vol. 69, No. 4, pp. 181s-185s.
- 21 Rokhlin, S. I., and Guu, A. C., 1993, "A Study of Arc Force, Pool Depression, and Weld Penetration during Gas Tungsten Arc Welding," *Welding Journal*, Vol. 72, No. 8, pp. 381s-390s.
- 22 Richardson, R. W., et al., 1984, "Coaxial Arc Weld Pool Viewing for Process Monitoring and Control," *Welding Journal*, Vol. 63, No. 3, pp. 43-50.
- 23 Brzakovic, D., and Khani, D. T., 1991, "Weld Pool Edge Detection for Automated Control of Welding," *IEEE Transactions on Robotics and Automation*, Vol. 7, No. 3, pp. 397-403.
- 24 Boyer, K. L., and Penix, W. A., 1992, "An Image Analysis System for Coaxially Viewed Weld Scenes," *Machine Vision and Applications*, Vol. 5, No. 4, pp. 277-293.
- 25 Pietrzak, K. A., and Packer, S. M., 1991, "Coaxial Vision-Based Weld Pool Width Control," *ASME Welding and Joining Processes*, E. Kannatey-Asibu, Jr., et al., eds., pp. 251-264.
- 26 Hoffman, T., 1991, "Real-Time Imaging for Process Control," *Advanced Material & Processes*, Vol. 140, No. 3, pp. 37-43.
- 27 Davies, E. R., 1990, *Machine Vision: Theory, Algorithms and Practicalities*, Chapter 5, Academic Press.
- 28 Astrom, K. J., and Wittenmark, B. W., 1990, *Computer Controlled System: Theory and Design*, 2nd ed., Prentice Hall.
- 29 Akaike, H., 1974, "A New Look at the Statistical Model Identification," *IEEE Transactions on Automatic Control*, Vol. 19, pp. 716-723.
- 30 Clarke, D. W., Mohtadi, C., and Tuffs, P. S., 1987, "Generalized Predictive Control," *Automatica*, Vol. 23, No. 2, pp. 137-160.